INSTITUTE OF PHYSICS PUBLISHING PHYSICS IN MEDICINE AND BIOLOGY

Phys. Med. Biol. **49** (2004) 4785–4798 PII: S0031-9155(04)79745-6

A modelling error approach for the estimation of optical absorption in the presence of anisotropies

Jenni Heino[1] **and Erkki Somersalo**[2]

[1] Helsinki University of Technology, Laboratory of Biomedical Engineering, PO Box 2200, FIN-02015 HUT, Finland
[2] Helsinki University of Technology, Institute of Mathematics, PO Box 1100, FIN-02015 HUT, Finland

E-mail: Jenni.Heino@hut.fi and Erkki.Somersalo@hut.fi

Received 23 April 2004, in final form 31 August 2004
Published 1 October 2004
Online at stacks.iop.org/PMB/49/4785
doi:10.1088/0031-9155/49/20/009

Abstract

Optical tomography is an emerging method for non-invasive imaging of human tissues using near-infrared light. Generally, the tissue is assumed isotropic, but this may not always be true. In this paper, we present a method for the estimation of optical absorption coefficient allowing the background to be anisotropic. To solve the forward problem, we model the light propagation in tissue using an anisotropic diffusion equation. The inverse problem consists of the estimation of the absorption coefficient based on boundary measurements. Generally, the background anisotropy cannot be assumed to be known. We treat the uncertainties in the background anisotropy parameter values as modelling error, and include this in our model and reconstruction. We present numerical examples based on simulated data. For reference, examples using an isotropic inversion scheme are also included. The estimates are qualitatively different for the two methods.

1. Introduction

Light propagation in biological tissues and the effect of tissue microstructure on light propagation have been studied recently for diagnostic and therapeutic applications in medicine. In this context, anisotropic light propagation, i.e., propagation of light that depends on the absolute direction in tissue, has received some interest. Although in several tissue types light propagation may be taken as isotropic, there are some tissue types where the anisotropic characteristics may be of significant order. Such tissue types include, e.g., skin, muscle, tendon, dentin and the white matter of the brain tissue.

The two most prevalent interactions of light in tissue are absorption and scattering. Significant absorbers in tissue include, e.g., water and haemoglobin. Scattering in tissue

is due, e.g., to boundaries such as cell membranes and organelles inside the cells. If the structures in tissue have a preferential orientation, it may result in anisotropic light propagation in the macroscopic scale. Often, anisotropic light propagation in biological tissues stems from fibrous or tubular structures in the tissue. In Nickell *et al* (2000) anisotropic light propagation in the human skin was measured, and the measurements and Monte Carlo simulations gave reason to believe that the anisotropy was caused by the preferential orientation of the collagen fibres in the skin. In Kienle *et al* (2003), anisotropic scattering was observed due to the orientation of the tubules in the human dentin, and in Marquez *et al* (1998) different optical absorption and scattering properties were measured depending on the relative orientation of the muscle fibres in chicken breast tissue.

In this paper, we investigate the effects of anisotropies from the point of view of image reconstruction in optical tomographic imaging (Arridge 1999, Nissilä *et al* 2004) of human tissues. In optical imaging, light of near-infrared wavelength is guided onto the surface of the body, often using optical fibres, and detected at several measurement locations around the body. In tomography the purpose is to reconstruct the spatial distribution of the optical properties inside the tissue based on the properties of the measured light. The potential applications of this modality include, e.g., detection of breast cancer (Dehghani *et al* 2003, Franceschini *et al* 1997, Pogue *et al* 2001) and detection and localization of problems in blood perfusion and oxygenation in the head of premature infants (Hebden *et al* 2002, 2004). In the case of tomographic imaging of the head, anisotropic effects in the white matter of the brain may be of significance, and hence modelling of anisotropies and consideration during image reconstruction may lead to a more accurate reconstruction.

For most tissue types, as light traverses through the tissue, it is multiply scattered. The strong scattering in the tissue renders the propagation of NIR light a diffusion-type process, and hence most approaches to image reconstruction in optical tomography rely on a diffusion model for the light propagation. A commonly used forward model in optical tomography is the isotropic diffusion equation, which is derived as an approximation from the equation for radiative transfer under certain conditions met in most biological tissues. To model anisotropic light propagation, in Heino and Somersalo (2002) and Heino *et al* (2003), an anisotropic diffusion equation was derived from the equation of radiative transfer. In this model, the diffusion coefficient has a tensor presentation. Another diffusion-like model for anisotropic light propagation, presented in Dagdug *et al* (2003), was based on the continuous-time random walk.

Generally, the inverse problem of optical tomography consists of the reconstruction of the spatial distributions of the internal absorption and scattering (or diffusion) coefficients based on the boundary measurements. This is an ill-posed inverse problem in the sense that small changes in the measured data can lead to arbitrary large changes in the estimated distribution. Reconstruction of the absorption and scalar diffusion coefficients is a challenging problem already; however, in the anisotropic case the number of unknown parameters is even larger. Using, e.g., the tensor presentation for the diffusion coefficient, both the principal directions of anisotropy and the strength of diffusion in these directions should be searched for. Generally, the anisotropy parameters cannot be assumed known, although in some cases one might have some prior information based on, e.g., knowledge of the anatomy or some other imaging modality such as the diffusion tensor magnetic resonance imaging (DTI) (Tuch *et al* 2001).

In Heino and Somersalo (2002), we have proposed a method based on a statistical approach to overcome the problem of the increasing number of unknown parameters in the reconstruction. In this approach, parameters were modelled as random variables with their relevant probability densities and the estimate for the sought parameter of primary interest

was obtained by firstly forming the posterior probability density for this parameter on condition of the measurement. Secondly, the parameters not well known and not of primary interest were integrated out from this distribution and a point estimate for the sought quantity was drawn. The method was implemented for the case where the strength of the anisotropy in one of the principal directions was assumed unknown and modelled using a rather wide probability distribution and the estimates for the absorption coefficient sought.

In this paper, we develop some of the ideas presented in Heino and Somersalo (2002) further. We present an approach for the image reconstruction, where one of the parameters, namely the absorption coefficient, is assumed to be the parameter of primary interest. The uncertainty in the values of the rest of the unknown parameters is treated as modelling error. By constructing a presentation for the measurements and the modelling error, information about the absorption coefficient can be retrieved with a weakly informative prior model of the anisotropy.

This paper is organized as follows. In section 2, we present the model for anisotropic light propagation with its numerical implementation. In section 3, we firstly define the inverse problem, and then introduce inversion schemes using the isotropic model and the anisotropic modelling error approach with some numerical examples. Finally, in section 4, we present conclusions and discussion.

2. Model for anisotropic light propagation

2.1. Anisotropic diffusion model

In optical tomography light propagation can generally be modelled using the transport theory (Chandrasekhar 1960, Ishimaru 1978), where the governing equation is the radiative transfer equation (RTE), also known as the Boltzmann equation. Numerical solutions to the RTE are rather tedious and involved, and therefore for image reconstruction approximations to the RTE are in practice used. When scattering dominates over absorption, the most commonly used approximation is the diffusion equation (DE), which is usually derived in its isotropic form.

The starting point in this paper is the anisotropic diffusion equation, which can be derived from the RTE in several ways (see, e.g., Heino and Somersalo (2002), Heino *et al* (2003)). In Heino *et al* (2003), the anisotropic DE was derived by constructing a model for anisotropic scattering by considering scattering from an infinite cylinder imitating the tubular structures met in some biological tissues. For a source modulated with an angular frequency ω, the anisotropic DE can be written as

$$-\nabla \cdot \mathsf{K}(\mathbf{r})\nabla\Phi(\mathbf{r}) + \left(\mu_{\mathrm{a}}(\mathbf{r}) - \frac{\mathrm{i}\omega}{c}\right)\Phi(\mathbf{r}) = q(\mathbf{r}), \tag{1}$$

where Φ is the complex fluence arising from the intensity modulated part q of the source term, μ_{a} is the absorption coefficient, c is the speed of light and K is the diffusion tensor

$$\mathsf{K} = \frac{1}{n}((\mu_{\mathrm{a}} + \mu_{\mathrm{s}})\mathsf{I} - \mu_{\mathrm{s}}\mathsf{B})^{-1}. \tag{2}$$

Above, μ_{s} is the scattering coefficient, n ($n = 2, 3$) is the dimension of the body Ω where the DE is solved and the anisotropic behaviour is confined in the matrix B. The elements of B can formally be obtained through integration of the so-called scattering phase function over the incident and scattered angles (Heino and Somersalo 2002). One may also consider that B is obtained by first forming a diagonal matrix with the so-called forward scattering biases (defined in connection of the diffusion approximation in, e.g., Heino *et al* (2003))

in each (n) orthogonal direction as the diagonal and successively rotating the matrix to get the relevant orientation. The isotropic case is obtained by setting the value of the forward scattering bias the same in all directions. Commonly, the isotropic case is presented using a scalar diffusion coefficient $\kappa = \frac{1}{n}(\mu_a + (1-b)\mu_s)^{-1}$, where b is the average value of the cosine of the scattering angle.

2.2. Source and boundary conditions

In this work, we model the light source as a collimated pencil beam perpendicular to the surface $\partial\Omega$ of the body. This model is often referred to as a collimated source approximation (Schweiger *et al* 1995). In practice, the source term is approximated by a point source below the surface: $q(\mathbf{r}) = q\delta(\mathbf{r} - \mathbf{r}_s)$, where $\mathbf{r}_s$ is the virtual source position. In order to derive the boundary condition, we assume that the inward directed current in each point on the boundary $\partial\Omega$ is zero. Within the diffusion approximation, this assumption leads to a so-called Robin boundary condition

$$\Phi + \frac{1}{2\gamma}\hat{n}\cdot \mathsf{K}\nabla\Phi = 0, \tag{3}$$

where $\hat{n}$ is the outward unit normal vector to the surface, the refractive index is assumed to be 1 and the constant $\gamma = \gamma_n$ depends on the dimension n and has values $\gamma_2 = 1/\pi$, $\gamma_3 = 1/4$. The boundary data consist of measured outward flux $\Phi_{\text{out}} = -\hat{n}\cdot\mathsf{K}\nabla\Phi$ at points $\mathbf{r}_m$, the optode locations, on the boundary $\partial\Omega$. Using the boundary condition (3), the outward flux can be calculated simply as $\Phi_{\text{out}}(\mathbf{r}_m) = 2\gamma\Phi(\mathbf{r}_m)$. Generally, measurement types are derived from the measured boundary flux to be used in image reconstruction. In this work, we use the natural logarithm of the amplitude $\ln A = \ln|\Phi_{\text{out}}|$ and the phase angle $\varphi = \arg\Phi_{\text{out}}$ of the complex boundary flux.

2.3. Numerical approximation

2.3.1. Presentation of the anisotropy in 2D. The numerical calculations in this work are conducted, solely for computational convenience, in a two-dimensional space. In 2D, we write the anisotropy matrix $\mathsf{B} \in \mathbb{R}^{2\times 2}$ as

$$\mathsf{B}(\mathbf{r}) = \mathsf{U}(\mathbf{r})\,\mathrm{diag}(b_1(\mathbf{r}), b_2(\mathbf{r}))\mathsf{U}(\mathbf{r})^{\mathrm{T}}, \tag{4}$$

where $\mathsf{U} \in \mathbb{R}^{2\times 2}$ is an orthogonal rotation matrix containing the information about the direction of the anisotropy, and the eigenvalues b_1 and b_2 are positive. The above form of the anisotropy matrix B leads to a similar formulation for the diffusion tensor K:

$$\mathsf{K}(\mathbf{r}) = \mathsf{U}(\mathbf{r})\,\mathrm{diag}(\lambda_1(\mathbf{r}), \lambda_2(\mathbf{r}))\mathsf{U}(\mathbf{r})^{\mathrm{T}}, \tag{5}$$

where

$$\lambda_j(\mathbf{r}) = \frac{1}{2(\mu_a(\mathbf{r}) + (1-b_j(\mathbf{r}))\mu_s(\mathbf{r}))}, \qquad j = 1, 2. \tag{6}$$

We denote the angle of the first eigenvector in the rotation matrix U by θ and use that as a parameter to indicate the direction of the anisotropy, i.e., we have

$$\mathsf{U}(\mathbf{r}) = (\bar{a}_1(\mathbf{r})\bar{a}_2(\mathbf{r})) = \begin{pmatrix} \cos\theta(\mathbf{r}) & -\sin\theta(\mathbf{r}) \\ \sin\theta(\mathbf{r}) & \cos\theta(\mathbf{r}) \end{pmatrix}. \tag{7}$$

The angle $\theta(\mathbf{r})$ is restricted in the interval $0 \leqslant \theta(\mathbf{r}) < \pi$. Observe that when the material is locally isotropic, that is, $\lambda_1(\mathbf{r}) = \lambda_2(\mathbf{r})$, the definition of the angle $\theta(\mathbf{r})$ becomes ambiguous.

2.3.2. Finite element method. The numerical approximation for the anisotropic DE is based on the finite element (FE) method. To implement the FE method, we first write the variational formulation of the anisotropic DE (1). By multiplying equation (1) by a test function ψ, integrating by parts over Ω, and including the Robin boundary condition (3) and the collimated source approximation, we arrive at the weak formulation: Find Φ such that

$$\int_\Omega \nabla\psi \cdot \mathsf{K}\nabla\Phi \,\mathrm{d}\mathbf{r} + \int_\Omega \left(\mu_\mathrm{a} - \frac{\mathrm{i}\omega}{c}\right)\psi\Phi \,\mathrm{d}\mathbf{r} + \int_{\partial\Omega} \frac{2}{\pi}\psi\Phi \,\mathrm{d}S = q\psi(\mathbf{r}_s) \tag{8}$$

$\forall\psi \in H^1(\Omega)$, where $H^1(\Omega)$ is a predefined function space (Sobolev space) for the test functions and the dimension-dependent constant $\gamma = \gamma_2 = 1/\pi$.

In the finite element approximation, the domain Ω is divided into finite elements and the solution is approximated by nodal-based basis functions,

$$\Phi(\mathbf{r}) \approx \sum_{j=1}^{N_\mathrm{n}} \alpha_j \psi_j(\mathbf{r}), \tag{9}$$

where N_n is the number of the nodes in the finite element mesh. By choosing the test function ψ in (8) to be one of the basis functions, we arrive at the matrix equation $A\alpha = \beta$, where A is the $N_\mathrm{n} \times N_\mathrm{n}$ symmetric matrix with entries

$$A_{j,\ell} = \int_\Omega \nabla\psi_j \cdot \mathsf{K}\nabla\psi_\ell \,\mathrm{d}\mathbf{r} + \int_\Omega \left(\mu_\mathrm{a} - \frac{\mathrm{i}\omega}{c}\right)\psi_j\psi_\ell \,\mathrm{d}\mathbf{r} + \int_{\partial\Omega} \frac{2}{\pi}\psi_j\psi_\ell \,\mathrm{d}S, \tag{10}$$

and β is an N_n-vector $\beta_j = q\psi_j(\mathbf{r}_s)$.

3. Inverse problem

3.1. Formulation of the inverse problem

The inverse problem we consider in this paper is the following: we assume that the absorption coefficient and the diffusion tensor in the domain (body) of interest Ω are unknown. The measurements on the boundary $\partial\Omega$ consist of frequency domain data $(\ln A, \varphi)$. The goal then is to estimate the spatial distribution of the absorption coefficient based on the boundary measurements. Note that the domain is not restricted to be anisotropic; part or all of it may be isotropic.

The motivation for this kind of formulation of the inverse problem comes from the consideration of the tomography of, e.g., the head of a premature infant, where the anisotropic structures in the white matter of the brain may affect light propagation. Some prior knowledge on the directions of the anisotropies may be extracted from anatomical information or other imaging modalities such as diffusion tensor MRI, but this information may not always be available or it may not be very accurate. Hence, in this paper, we assume that our prior knowledge consists of, e.g., information on the typical ranges of the absorption and/or scattering coefficient in biological tissues. At this point, also, it is worth noting that though it has been verified by Monte Carlo simulations that structural anisotropy seems to give rise to anisotropic light propagation, to our knowledge, neither anisotropic light propagation in the white matter of the brain nor the correlation between the optical and (water) diffusion anisotropies has been experimentally verified. Also, considering, e.g., optical imaging of the neonatal head, the first reconstructions based on real data have been published only recently (Hebden *et al* 2002, 2004). In previous studies (Heino and Somersalo 2002, Heino *et al* 2002), it has been demonstrated with numerical simulations that if the anisotropic effect in light propagation is significant, including the anisotropy in the reconstruction model improves the results. Whether the anisotropy is significant in real measurements remains to be seen.

The observation model used in this work is

$$y = G(\mu_a, \lambda_1, \lambda_2, \theta) + n, \tag{11}$$

where y is a vector consisting of the values of the measured quantities (logarithm of the amplitude and phase angle) on the measurement points, $G(\mu_a, \lambda_1, \lambda_2, \theta)$ is the model of the noiseless observation and n is additive measurement noise. In the isotropic case, the corresponding observation model is $y = G(\mu_a, \kappa) + n$.

3.2. Solution by isotropic and fixed anisotropic models

In this section, we present two examples of image reconstruction. The first straightforward attempt for image reconstruction might be to use an isotropic model, or, alternatively, to make a guess of at least some of the anisotropic properties in the domain and use this partly fixed model in the reconstruction. For reference, we include here a reconstruction in both of the above manners.

The first reconstruction is performed using an isotropic model and a truncated Levenberg–Marquardt (LM) iteration (see, e.g., Dennis and Schnabel (1996)) for the estimation of μ_a. To aid the reconstruction, estimation of κ is also included. The Levenberg–Marquardt method is an iterative method for minimizing the mean square error $\|y - G(\mu_a, \kappa)\|^2$ by local linearizations. If $\left(\mu_a^j, \kappa^j\right)$ is the current estimate of the unknown parameters μ_a and κ, we write the local linearization of the observation model as

$$G(\mu_a, \kappa) = G\left(\mu_a^j + \delta\mu_a, \kappa^j + \delta\kappa\right) \approx G\left(\mu_a^j, \kappa^j\right) + J_{\mu_a}^j \delta\mu_a + J_\kappa^j \delta\kappa,$$

where $J_{\mu_a}^j$ and J_κ^j denote the Jacobians of the mapping G with respect to μ_a and κ, respectively, calculated at the current estimate. The LM iteration step $\left(\mu_a^j, \kappa^j\right) \to \left(\mu_a^{j+1}, \kappa^{j+1}\right) = \left(\mu_a^j + \delta\mu_a, \kappa^j + \delta\kappa\right)$ comprises the minimization of a functional of the form

$$\mathcal{F}(\delta\mu_a, \delta\kappa) = \left\| y - \left(G\left(\mu_a^j, \kappa^j\right) + J_{\mu_a}^j \delta\mu_a + J_\kappa^j \delta\kappa\right)\right\|^2 + \rho(\|\delta\mu_a\|^2 + \|\delta\kappa\|^2),$$

where ρ is a local regularization parameter.

In this work, we use only a single local regularization parameter ρ. This is justified since the parameters μ_a and κ have been scaled to be of the same order of magnitude. Having different parameters multiplying the norms of $\delta\mu_a$ and $\delta\kappa$ would give more flexibility but also the judicious selection of these parameters becomes more complicated. In classical LM literature (see, e.g., Dennis and Schnabel (1996)), the selection of the parameter ρ is based on trust region considerations. Here, it is selected by visual inspection.

The minimization procedure is performed in two stages. First, the scalar background values for μ_a and κ were searched for by performing a few steps of the LM iteration until these values converged. The iteration is then changed into pixel basis, where each parameter has a constant value in each element of the FE mesh.

Observe that when pixel-based representations are used, due to the ill-posedness of the inverse problem and the presence of noise and modelling errors, the LM method does not guarantee convergence to anything useful. Indeed, continuing the iterations, the method fits the model to the noise and the outcome is a noise image. Therefore, in addition to the local regularization of the iteration step, one needs to include a global regularization scheme. Here the regularization is done by simply truncating the iteration process prior to convergence.

Figure 1 shows the geometry of the test case used for the calculation of the data. The data were created with a different mesh than that used for the reconstruction. The forward and inverse meshes consisted of 7014 and 2993 elements, respectively, and had been created with a bubble mesh generator (Järvenpää 2001). For the amplitude, the relative noise level

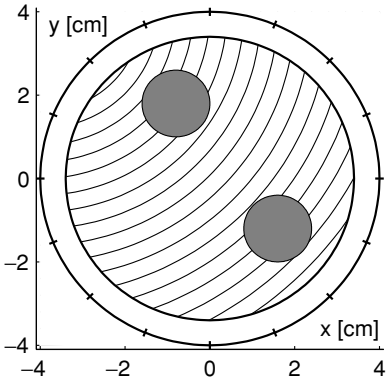

Figure 1. The 2D model used for data generation. The boundary of the domain is isotropic with $\kappa = 0.0500\ \mathrm{cm}^{-1}$ and the central striped part anisotropic with the direction of anisotropy parallel to the stripes and $(\lambda_1, \lambda_2) = (0.0500\ \mathrm{cm}^{-1},\ 0.0167\ \mathrm{cm}^{-1})$. The background absorption $\mu_{\mathrm{a,bg}} = 0.10\ \mathrm{cm}^{-1}$ and the two grey spheres (radii 0.8 cm) represent two perturbations in the absorption coefficient with $\mu_{\mathrm{a}} = 0.20\ \mathrm{cm}^{-1}$. Simulated data were collected using 16 source/measurement locations at equal distances on the boundary. The source is placed at each location in turn, and the rest of the locations are used for measurement, resulting in 240 data values for each measurement type.

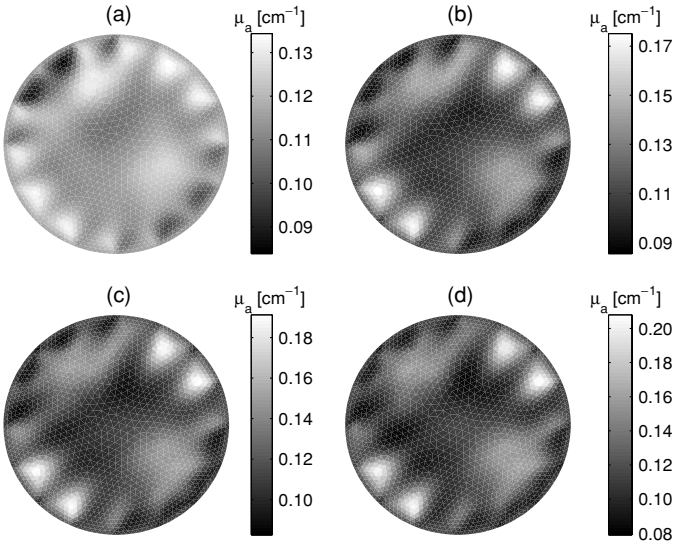

Figure 2. Reconstruction of the absorption coefficient using the isotropic model at different stages of the iteration: (a) first iteration, (b) fifth iteration, (c) 10th iteration and (d) 20th iteration.

was assumed to be $\sim$1%, and for the phase, the noise was assumed to have a level of $\sim 1^{\circ}$. Artificial noise corresponding to these levels was added to the computed signal.

Figure 2 displays reconstructions of the absorption coefficient at different stages of the iteration, up to 20 iterations. The initial value of the iteration for μ_{a} was $\mu_{\mathrm{a},0} = 0.05\ \mathrm{cm}^{-1}$. For the diffusion coefficient κ, the initial value was equal to the value of κ in the isotropic part of the disc in figure 1. Albeit not very clear, the estimate of the absorption coefficient indicates inhomogeneities at correct positions. As the iteration proceeds, the method starts

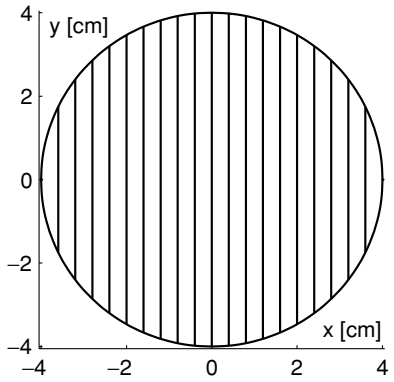

Figure 3. The anisotropic model used as a starting point of the reconstruction. The direction of anisotropy is parallel to the y-axis ($\theta = 90^\circ$), the strength of anisotropy $(\lambda_1, \lambda_2) = (0.0333\ \mathrm{cm}^{-1}, 0.0250\ \mathrm{cm}^{-1})$ and the absorption coefficient $\mu_\mathrm{a} = 0.05\ \mathrm{cm}^{-1}$.

to fit increasingly the model to the modelling error that is predominant in comparison to the artificial noise. Consequently, the reconstructions start to be dominated by the artefacts near the measurement point. The moderate success of the algorithm, at least at low iteration counts, is based on the partial compensation of the effects of anisotropy by heavy artefacts on the estimate κ on the boundary. Indeed, if κ is not included in the reconstruction but fixed, e.g., to the true boundary value, nothing sensible is visible in the estimate of μ_a. The reconstruction of κ is useless here and therefore we have not displayed it.

The second reconstruction was done using a partly fixed anisotropic model and the truncated Levenberg–Marquardt iteration. The data were calculated again as described above, using the geometry displayed in figure 1. The model for the anisotropic diffusion tensor is shown in figure 3. The direction of the anisotropy is fixed parallel to the y-axis. The strength parameters λ_1 and λ_2 are assumed to be spatially constant but unknown, so they are part of the reconstruction problem. In the LM iteration step $\left(\mu_\mathrm{a}^j, \lambda_1^j, \lambda_2^j\right) \to \left(\mu_\mathrm{a}^{j+1}, \lambda_1^{j+1}, \lambda_2^{j+1}\right)$, we minimize the functional

$$\mathcal{F}(\delta\mu_\mathrm{a}, \delta\lambda_1, \delta\lambda_2) = \left\| y - \left(G\left(\mu_\mathrm{a}^j, \lambda_1^j, \lambda_2^j\right) + J_{\mu_\mathrm{a}}^j \delta\mu_\mathrm{a} + J_{\lambda_1}^j \delta\lambda_1 + J_{\lambda_2}^j \delta\lambda_2 \right) \right\|^2 + \rho(\|\delta\mu_\mathrm{a}\|^2 + \|\delta\lambda_1\|^2 + \|\delta\lambda_2\|^2),$$

where, again, the Jacobians at the current estimate with respect to the estimated parameters appear. The starting point is again $\mu_{\mathrm{a},0} = 0.05\ \mathrm{cm}^{-1}$, and for λ_k, $(\lambda_{1,0}, \lambda_{2,0}) = (0.0333\ \mathrm{cm}^{-1}, 0.0250\ \mathrm{cm}^{-1})$. The LM iteration is done again in two steps, first by fitting the best constants and then using pixel-based representation for μ_a with iteration truncation. The reconstruction of the absorption coefficients after one pixel-based LM iteration is displayed in figure 4. The estimate is completely dominated by the artefacts that compensate the incorrectly modelled anisotropic structure. The iteration does not improve the estimate; in contrast, the artefacts become even more dominant.

The estimated κ in the former reconstruction and the strength parameters in the latter, although of interest in practice, are not considered in this work. Isotropic κ is firstly not properly defined in the anisotropic case, and secondly, the estimate is dominated by artefacts. As for the strength parameters, it is our experience that to obtain useful estimations, one should have a better prior model for the anisotropy parameters than the crude one we use here.

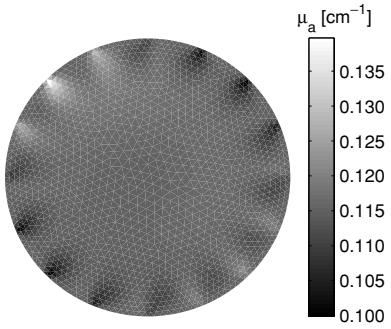

Figure 4. Reconstruction of the absorption coefficient using the partly fixed anisotropic model: first iteration.

3.3. Anisotropy as a modelling error

As the examples in the previous section show, reconstruction of the absorption coefficient in the presence of background anisotropies suffers dramatically, if the anisotropies are not modelled or if the model used is not truthful. However, in general we cannot assume to have precise knowledge of the anisotropy at hand. To overcome this problem, we now present an approach for estimating the optical properties of the body, where, following the Bayesian interpretation, the uncertainty in some of the parameter values is modelled. Here, we treat the uncertainties in the anisotropy parameters as modelling errors which are taken into account in the reconstruction.

Consider the observation model

$$y = G(\mu_a, \lambda_1, \lambda_2, \theta) + n.$$

We treat the absorption coefficient μ_a as the unknown of primary interest while the remaining parameters λ_1, λ_2 and θ are parameters of secondary interest.

Assume that we have preliminary estimates λ_1^*, λ_2^* and θ^* for these parameters. We write the model as

$$\begin{aligned} y &= G(\mu_a, \lambda_1^*, \lambda_2^*, \theta^*) + (G(\mu_a, \lambda_1, \lambda_2, \theta) - G(\mu_a, \lambda_1^*, \lambda_2^*, \theta^*)) + n \\ &= G(\mu_a, \lambda_1^*, \lambda_2^*, \theta^*) + \epsilon(\mu_a, \lambda_1, \lambda_2, \theta) + n. \end{aligned} \tag{12}$$

The term ϵ above is an error term that is non-vanishing if our estimates for the parameters do not coincide with the true values. It is our aim to treat the modelling error as noise.

Assume that we have specified the prior information of the variables $x \in S = \{\mu_a, \lambda_1, \lambda_2, \theta\}$. Then, it is possible in principle to determine the probability distribution of the modelling error ϵ. The complexity of this task depends on the form of the mapping G as well as on the prior distributions of the variables. In general, one has to use Monte Carlo methods for exploring the density (see Kaipio and Somersalo (2004)). An extra difficulty is due to the fact that the modelling error is statistically dependent on the variable μ_a that we want to estimate.

The problem becomes particularly simple if the mapping G is linear and the prior densities are Gaussian. We propose an iterative method based on local linearizations and Gaussian approximations that render the problem to the simple case. Let μ_a^j denote the current approximation of the absorption coefficient, $\mu_a^0 = \mu_a^*$. To approximate the modelling error term, we write first a local linearization

$$\epsilon(\mu_a, \lambda_1, \lambda_2, \theta) \approx \epsilon\big(\mu_a^j, \lambda_1, \lambda_2, \theta\big) \approx J_{\lambda_1}^j \delta\lambda_1 + J_{\lambda_2}^j \delta\lambda_2 + J_\theta^j \delta\theta,$$

where $\delta\lambda_k = \lambda_k - \lambda_k^*$, $k = 1, 2$, $\delta\theta = \theta - \theta^*$, and $J_{\lambda_k}^j$ and J_θ^j are the corresponding Jacobians at the estimators λ_k^* and θ^* with $\mu_a = \mu_a^j$. Hence, the total error term is approximately

$$e = \epsilon + n \approx J_{\lambda_1}^j \delta\lambda_1 + J_{\lambda_2}^j \delta\lambda_2 + J_\theta^j \delta\theta + n.$$

If we approximate the prior densities of the parameters by Gaussian densities,

$$x \sim \mathcal{N}(x^*, \Gamma_x), \qquad x = \lambda_1, \lambda_2 \text{ or } \theta,$$

and assume that the additive noise is independent of the parameters, the noise covariance becomes

$$\Gamma_e = \mathrm{E}\{ee^{\mathrm{T}}\} \approx J_{\lambda_1}^j \Gamma_{\lambda_1} \big(J_{\lambda_1}^j\big)^{\mathrm{T}} + J_{\lambda_2}^j \Gamma_{\lambda_2} \big(J_{\lambda_2}^j\big)^{\mathrm{T}} + J_\theta^j \Gamma_\theta \big(J_\theta^j\big)^{\mathrm{T}} + \Gamma_n = \Gamma_e^j.$$

The corresponding weighted mean square error is then

$$\begin{aligned} R^j(\mu_a) &= (y - G(\mu_a, \lambda_1^*, \lambda_2^*, \theta^*))^{\mathrm{T}} \big[\Gamma_e^j\big]^{-1} (y - G(\mu_a, \lambda_1^*, \lambda_2^*, \theta^*)) \\ &= \|y - G(\mu_a, \lambda_1^*, \lambda_2^*, \theta^*)\|_{\Gamma_e^j}^2. \end{aligned}$$

As in the previous section, we apply the LM iteration in two stages to minimize this expression, truncating the pixel-based iteration prior to convergence in order to regularize the ill-posedness. We minimize the quadratic functional

$$\mathcal{F}(\delta\mu_a) = \big\| y - \big(y^j + J_{\mu_a}^j \delta\mu_a\big) \big\|_{\Gamma_e^j}^2 + \rho \|\delta\mu_a\|^2,$$

where $J_{\mu_a}^j$ is the Jacobian of the mapping $\mu_a \mapsto G(\mu_a, \lambda_1^*, \lambda_2^*, \theta^*)$ at the current estimate μ_a^j.

A comment concerning the use of the LM iteration is in order. Statistically, the current approach is essentially a maximum likelihood estimation with regularization. In a purely Bayesian approach, the regularization by truncation is not needed, if we include an informative prior for μ_a into the object functional (see Kaipio and Somersalo (2004)). Here, we have avoided that firstly to obtain a fair comparison with the previously computed examples and secondly because we do not want to assume too much information about μ_a prior to the measurement, i.e., the prior is assumed to be flat.

Next we illustrate this method by some numerical examples. In the first example, the data used are the same as in previous examples, i.e., calculated with the model described in figure 1. To implement the numerical examples, we first need to set up the prior distributions $\mathcal{N}(x^*, \Gamma_x)$, $x \in \{\lambda_1, \lambda_2, \theta\}$. Let us now assume that all parameters $\{\lambda_1, \lambda_2, \theta\}$ are piecewise constant with constant values in each element of FE mesh. As the centre of the distribution, which signifies the *a priori* most probable value, we use the anisotropic background of figure 3. The prior covariance matrices are assumed to be $\Gamma_x = \sigma_x^2 I$, where the standard deviation σ_x of the variable $x \in S$ is constant.

We assume that our prior is not very informative, meaning that the prior variances are large. This assumption allows the true parameter values to lie far away from the centre $(\lambda_1^*, \lambda_2^*, \theta^*)$, which is the case in the simulation here. In practice, the values for the σ_x were selected using an 'ad hoc' method by firstly considering a relatively large interval in which the parameter value may lay and secondly defining the value of σ_x by considering a Gaussian distribution in this interval and requiring that the parameter value lies within this interval with a probability of 0.9–0.99 depending on the parameter. From the noise induced artificially into the measurement type $\ln A$, the value for $\sigma_{\ln A}$ was estimated to be $\sim$0.01. However, in practice a larger value helped improve the results. The values used in the calculations are listed in table 1. The reconstruction of the absorption coefficient is displayed in figure 5. In practice, the estimate was obtained by firstly estimating the background absorption $\mu_{a,bg}$ by

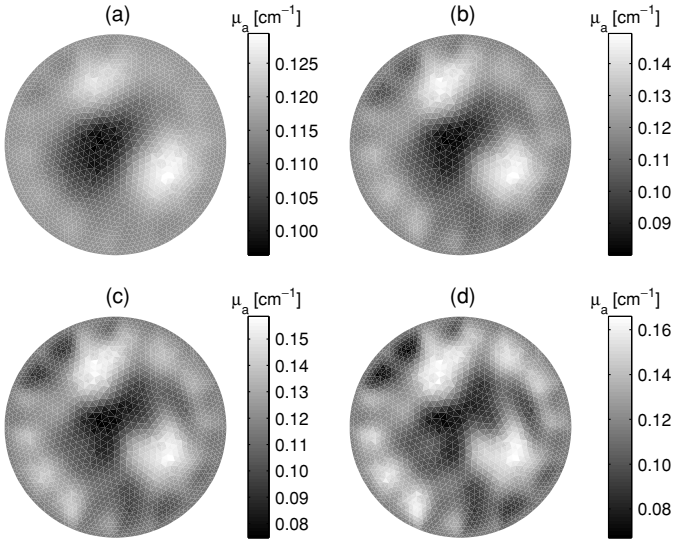

Figure 5. Reconstruction of the absorption coefficient with the modelling error approach at different stages of the iteration: (a) first iteration, (b) fifth iteration, (c) 10th iteration and (d) 20th iteration.

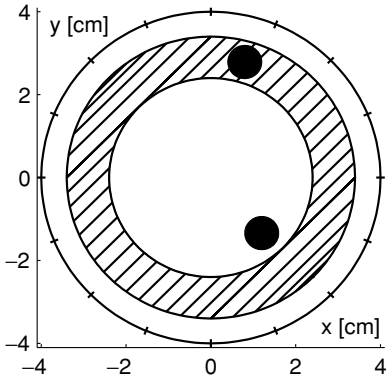

Figure 6. The second model used for data generation. In the anisotropic ring (striped area), $\theta = 45^\circ$ and $(\lambda_1, \lambda_2) = (0.0500\ \mathrm{cm}^{-1}, 0.0167\ \mathrm{cm}^{-1})$. The rest of the disc is isotropic with $\kappa = 0.0500\,\mathrm{cm}^{-1}$. In the background, $\mu_{\mathrm{a,bg}} = 0.1\ \mathrm{cm}^{-1}$ and in the spherical perturbations (black, radii 0.4 cm), $\mu_{\mathrm{a}} = 0.25\ \mathrm{cm}^{-1}$.

Table 1. The parameter values used for the reconstruction in modelling error approach.

$\lambda_1^* = 0.0333\ \mathrm{cm}^{-1}$	$\sigma_{\lambda_1} = 0.020\ \mathrm{cm}^{-1}$
$\lambda_2^* = 0.0250\ \mathrm{cm}^{-1}$	$\sigma_{\lambda_2} = 0.020\ \mathrm{cm}^{-1}$
$\theta^* = \pi/2$ rad	$\sigma_\theta = 0.68$ rad
$\mu_{\mathrm{a}}^* = 0.050\ \mathrm{cm}^{-1}$	$\sigma_{\ln A} = 0.07$
	$\sigma_\varphi = 0.0175$ rad

applying the LM iteration solely on the scalar μ_{a} with λ_1 and λ_2 constants. Secondly, all parameters $\{\mu_{\mathrm{a}}, \lambda_1, \lambda_2, \theta\}$ were assumed spatially variant (piecewise constant) as described above. After a few iterations, the inhomogeneities can be seen much more clearly than without

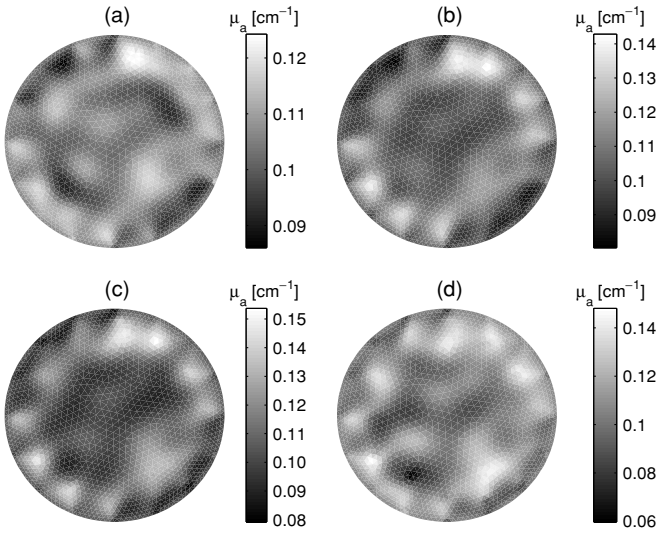

Figure 7. Reconstruction of the absorption coefficient with the isotropic model at different stages of the iteration: (a) first iteration, (b) fifth iteration, (c) 10th iteration and (d) 20th iteration.

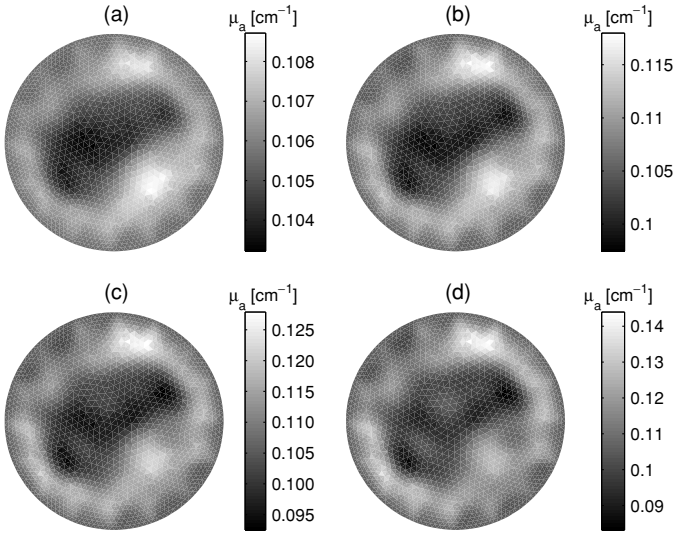

Figure 8. Reconstruction of the absorption coefficient with the modelling error approach at different stages of the iteration: (a) first iteration, (b) fifth iteration, (c) 10th iteration and (d) 20th iteration.

the modelling error approach in figure 2. As the iteration proceeds, the modelling artefacts start to increase here, too, although not taking over as badly as in the previous case.

As the second example, we consider an anisotropic ring located inside an isotropic disc. The model used the data calculation described in detail in figure 6. Artificial measurement noise corresponding to noise levels of $\sim$1% for the amplitude and $\sim 1^\circ$ for the phase was again added to the data. The reconstruction was performed with both the isotropic LM iteration and the LM iteration with the modelling error approach in the same way as in the first example. The reconstructions of μ_a are plotted in figures 7 and 8. In this case, the estimates of the

inclusions are less clear. This result could be expected, since the inclusions are small and consequently, any inversion method has more difficulty in resolving the anomalies.

4. Conclusions and discussion

In this paper, we have presented an approach for the estimation of the absorption coefficient, in which the background anisotropy is included in the model as a modelling error. This resulted in qualitatively different images in terms of less boundary artefacts compared to those obtained using a conventional isotropic inversion scheme.

The parameter of primary interest was considered to be the absorption coefficient. However, in principle the method presented in this paper could be applied to the estimation of the anisotropy parameters as well. The inverse problem of determining the anisotropic structures of the body is a challenging problem with potential applications, e.g., in studying the connectivity of the brain. The optical information may provide complementary information to that obtained for example with DTI. To be more precise, the estimates of optical anisotropy can be used to answer the question: to what extent do the optical and diffusive properties of the tissue correlate? This in turn is important when different measurement modalities are used simultaneously. In this work, the anisotropy in the inverse problem employing the modelling error approach was modelled by a pixel-based model, where the values in each pixel were uncorrelated. In order to improve the estimates of the absorption, as well as the estimation of the anisotropy in view, however, there are several questions that need to be considered. First, in a structured body such as the human brain, the anisotropy directions are correlated, and this correlation should be coded into the prior density. Second, as was mentioned, when the material is locally isotropic, the definition of the anisotropy angle becomes ambiguous. This shows up as severe instability of the estimates. Preliminary experiments without proper modelling of these features result in reconstructions that are not very informative.

One of the central questions to be resolved in future work is the modelling of linearization errors, or, alternatively, the development of a fully non-linear inversion method for anisotropic media. In the present work, linearization for the anisotropy parameters was used. From numerical experiments, however, this linearizing error was found to be up to two orders larger than the applied additive noise. This modelling error was compensated by overregularizing during the estimation of the absorption coefficient. Such a procedure may lead to useful images, as we demonstrated, but it affects the dynamical range of the reconstruction.

Acknowledgments

This work was supported by the Academy of Finland, the Graduate School Functional Research in Medicine and the Emil Aaltonen Foundation. The authors thank I Nissilä MSc for careful reading of the manuscript.

References

Arridge S R 1999 Optical tomography in medical imaging *Inverse Problems* **15** R41–93

Chandrasekhar S 1960 *Radiative Transfer* (New York: Dover)

Dagdug L, Weiss G H and Gandjbakhche A H 2003 Effects of anisotropic optical properties on photon migration in structured tissues *Phys. Med. Biol.* **48** 1361–70

Dehghani H, Pogue B W, Poplack S P and Paulsen K D 2003 Multiwavelength three-dimensional near-infrared tomography of the breast: initial simulation, phantom, and clinical results *Appl. Opt.* **42** 135–45

Dennis J E and Schnabel R B 1996 *Numerical Methods for Unconstrained Optimization and Nonlinear Equations (Classics in Applied Mathematics* vol 16*)* (Philadelphia, PA: SIAM)

Franceschini M A, Moesta K T, Fantini S, Gaida G, Gratton E, Jess H, Mantulin W W, Seeber M, Schlag P M and Kaschke M 1997 Frequency-domain techniques enhance optical mammography: initial clinical results *Proc. Natl Acad. Sci. USA* **94** 6468–73

Hebden J C, Gibson A, Austin T, Yusof R, Everdell N, Delpy D T, Arridge S R, Meek J H and Wyatt J S 2004 Imaging changes in blood volume and oxygenation in the newborn infant brain using three-dimensional optical tomography *Phys. Med. Biol.* **49** 1117–30

Hebden J C, Gibson A, Yusof R M, Everdell N, Hillman E M C, Delpy D T, Arridge S R, Austin T, Meek J H and Wyatt J S 2002 Three-dimensional optical tomography of the premature infant brain *Phys. Med. Biol.* **47** 4155–66

Heino J, Arridge S, Sikora J and Somersalo E 2003 Anisotropic effects in highly scattering media *Phys. Rev.* E **68** 031908

Heino J and Somersalo E 2002 Estimation of optical absorption in anisotropic background *Inverse Problems* **18** 559–73

Heino J, Somersalo E and Arridge S 2002 Simultaneous estimation of optical anisotropy and absorption in medical optical tomography *Proc. 4th Int. Workshop Computational Problems of Electrical Engineering (Zakopane, Poland 2–5 Sept. 2002,)* pp 191–4

Ishimaru A 1978 *Wave Propagation and Scattering in Random Media, Vol 1 Single Scattering and Transport Theory* (New York: Academic)

Järvenpää S 2001 Implementation of PML absorbing boundary condition for solving Maxwell's equations with Whitney elements *PhD Thesis* University of Helsinki

Kaipio J and Somersalo E 2004 *Statistical and Computational Inverse Problems* (Berlin: Springer) at press

Kienle A, Forster F K, Diebolder R and Hibst R 2003 Light propagation in dentin: influence of microstructure on anisotropy *Phys. Med. Biol.* **48** N7–14

Marquez G, Wang L V, Lin S, Schwartz J A and Thomsen S L 1998 Anisotropy in the absorption and scattering of chicken breast tissue *Appl. Opt.* **37** 798–804

Nickell S, Hermann M, Essenpreis M, Farrell T J, Krämer U and Patterson M S 2000 Anisotropy of light propagation in human skin *Phys. Med. Biol.* **45** 2873–86

Nissilä I, Noponen T, Heino J, Kajava T and Katila T 2004 Diffuse optical imaging ed J Lin *Advances in Electromagnetic Fields in Living Systems* vol 4 (New York: Kluwer) at press

Pogue B W, Poplack S P, McBride T O, Welss W A, Osterman K S, Ostenberg U L and Paulsen K D 2001 Quantitative hemoglobin tomography with diffuse near-infrared spectroscopy: pilot results in the breast *Radiology* **218** 261–6

Schweiger M, Arridge S R, Hiraoka M and Delpy D T 1995 The finite element method for the propagation of light in scattering media: boundary and source conditions *Med. Phys.* **22** 1779–92

Tuch D S, Wedeen V J, Dale A M, George J S and Belliveau J W 2001 Conductivity tensor mapping of the human brain using diffusion tensor MRI *Proc. Natl. Acad. Sci. USA* **98** 11697–701